

Structure–activity studies of ferroelectric and antiferroelectric imine ligands and their palladium(II) complexes. An antiferroelectric metallomesogen

Delia López de Murillas,^a Rafael Piñol,^a M. Blanca Ros,^a José Luis Serrano,^{*a} Teresa Sierra^a and M. Rosario de la Fuente^b

^aQuímica Orgánica, Facultad de Ciencias-I.C.M.A., Universidad de Zaragoza-C.S.I.C., 50009-Zaragoza, Spain

^bDept. Física Aplicada II, Facultad de Ciencias, Universidad del País Vasco, Aptdo. 644, 48080-Bilbao, Spain

Received 8th September 2003, Accepted 7th January 2004

First published as an Advance Article on the web 20th February 2004

The synthesis and characterization of the mesomorphic and dielectric properties of new imine-based liquid crystalline compounds that exhibit tilted SmC* phases is reported. The presence of an imino linkage within the mesogenic nucleus of these compounds is significant due to the ability of benzaldimines to coordinate to metals. Complexation to a divalent metal such as Pd(II) has been studied in order to assess the effects of antiparallel dimerization of organic ligands, through metal-coordination, on the appearance of antiferroelectric order in the mesophase. An organometallic palladium(II) complex has been prepared and this shows antiferroelectric behaviour over the whole range of the tilted smectic mesophase. Structure–activity studies have also been carried out by varying structural elements in the composition of the ligands. The changes include the disposition of the linking groups within the mesogenic core, and presence of a lateral hydroxy group.

Introduction

Interest in Antiferroelectric Liquid Crystals (AFLCs) is based on their characteristic features and, in particular, on new effects, such as thresholdless antiferroelectricity or V-shaped switching – properties that make these systems suitable materials for flat panel displays.¹ Since the first confirmation of this property,² the need for suitable materials has led to the design and synthesis of many calamitic molecules, most of which are structurally related to the first AFLC, MHPOBC. Structure–activity studies have been carried out in an attempt to establish the molecular characteristics required for the appearance of antiferroelectric order in the mesophase. The most significant conclusions indicate a molecule consisting of a three-ring core, with at least two aromatic rings that are not directly connected, and a chiral tail with a transversal disposition with respect to the long molecular axis and connected to the rigid core through a carboxylate linkage.³ The main types of connectors within the core have been dipole-associated functional groups such as ester or amido groups.

Examination of the crystalline structures of mesogenic compounds exhibiting antiferroelectric behavior⁴ shows that molecules adopt a herringbone crystal packing with a layer-like organization. Within each layer, mesogenic moieties adopt an antiparallel arrangement with the chiral tail almost perpendicular to the core moiety. Additionally, two ester groups of each molecule are oriented in the same direction transversal to the long molecular axis, making the layer highly polar with additional ester–ester interactions. These structures have been interpreted as being responsible for antiferroelectric ordering within the liquid crystal phase, a situation in which interlayer interactions would be stabilized by an alternating arrangement of highly polar layers.

The work described here deals with the synthesis and the liquid crystal and dielectric characterization of different imine derivatives whose molecular structure is based on the generally accepted formula reported for antiferroelectric mesogenic

molecules. Furthermore, these imino compounds possess the ability to coordinate to metals. The aforementioned antiparallel arrangement in the crystal is reminiscent of the ligand disposition in the square-planar dimeric metal complexes derived from Schiff bases (Fig. 1), investigated in depth by our group.⁵ On the basis of this structural similarity we were tempted to investigate the possibilities for metal complexation of our chiral imines with the aim of inducing or stabilizing antiferroelectric order in metallomesogens. Such structures

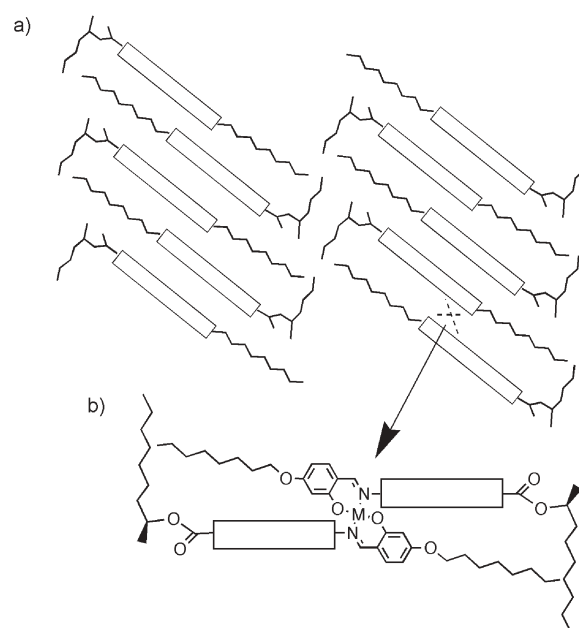


Fig. 1 a) Schematic representation of the crystal structure of a typical antiferroelectric liquid crystal according to ref. 4d. b) The antiparallel disposition of the molecules is reminiscent of the ligand orientation in square-planar dimeric Schiff base complexes. As an example, the general structure of a salicylaldehyde is represented in the figure.

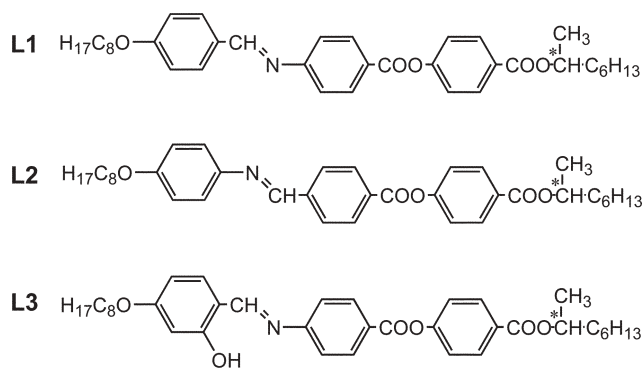


Chart 1

have no precedents in the literature. Metal complexation could well prove to be a convenient approach to new antiferroelectric materials.

For this purpose, we designed organic ligands that structurally have the capability to coordinate to metal atoms and also incorporate a chiral tail and linkages that favor highly polar layers and, hence, promote antiferroelectric order within the mesophase (Chart 1). From these ligands, we selected different square-planar dimeric structures, namely palladium(II) salicylaldimines and acetato- and chloro-bridged-*ortho*-palladated structures that ensure a fixed antiparallel, *i.e.* *trans*, disposition of the ligands within the complex (Chart 2).

In order to gain an insight into the molecular structural factors that influence the appearance of either ferro- or antiferro-electric order, or both, in the ligands and the metal complexes, we prepared three types of chiral Schiff base ligand. All of them consist of a three-ring mesogenic core in which the aromatic rings are linked by two different groups, *i.e.* an imino

and an ester group – the former has scarcely been employed in the design of antiferroelectric liquid crystals.⁶ Structural modifications were also undertaken, and these included: (i) the relative orientation of the dipoles along the longitudinal molecular axis (**L1** vs. **L2**), (ii) the presence of lateral polar groups such as a hydroxy group, which can affect the rigidity and polarisability of the mesogenic nucleus by means of intramolecular hydrogen-bonding (**L3** vs. **L1**) and will allow a different way of chelation to the metal atom.

Coordination of salicylaldimine **L3** to Pd(II) gives rise to a square-planar dimeric complex through chelation of the N (imine) and O (hydroxy group) heteroatoms to the metal. The resulting molecular structure consists of two ligands whose mesogenic moieties face each other and adopt an antiparallel disposition of their mesogenic nuclei fixed by coordination to the metal. Likewise, orthopalladation complexes derived from benzaldimines **L1** and **L2** and their reaction with palladium(II) acetate, and these with palladium(II) chloride, give rise to dimeric dinuclear complexes. In this case the antiparallel orientation of the ligands is only achieved if the coordination to the metal occurs with a *trans* configuration of the chelating atoms. This situation can be readily confirmed by ¹H NMR, as already reported for various examples.⁷ Taking into account the conformation of this type of ligand in which the chiral tail adopts a disposition almost perpendicular to the rest of the molecule,⁴ the final molecular shape of all these complexes is reminiscent of the crystal packing described for some liquid crystals that exhibit the antiferroelectric SmC*_A mesophase, as mentioned above.

All of the compounds were studied by optical microscopy, DSC and broadband dielectric spectroscopy. The spontaneous polarisation values were evaluated by means of the triangular wave method, wherever possible.

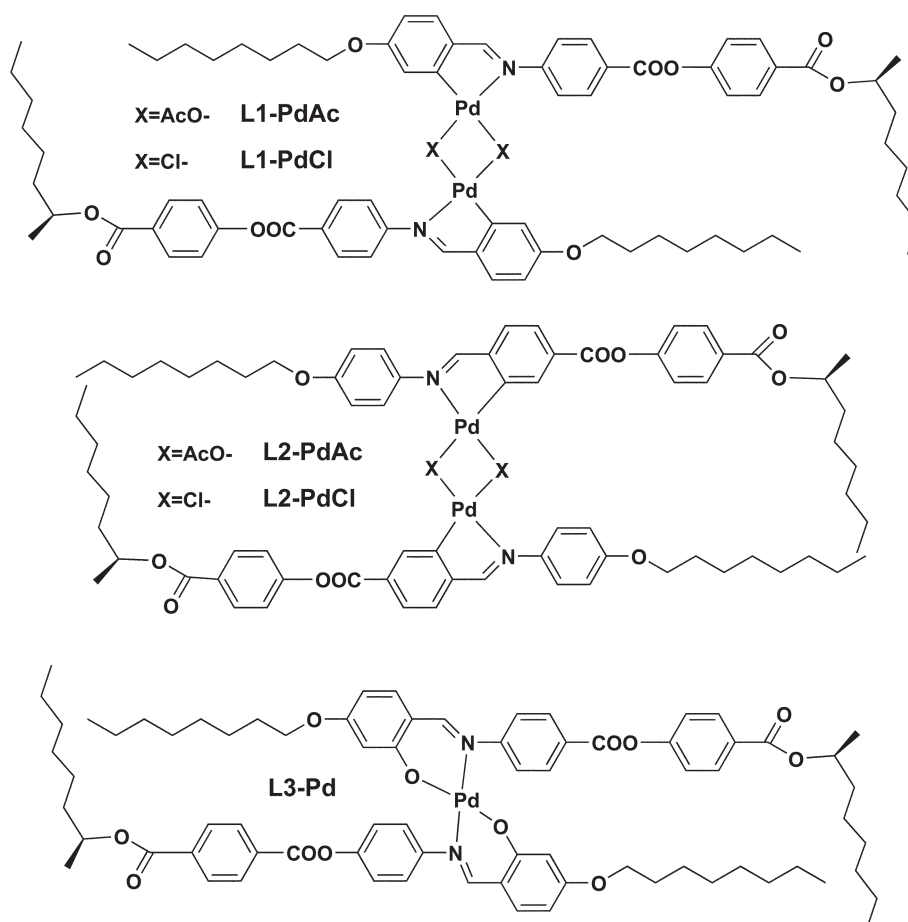
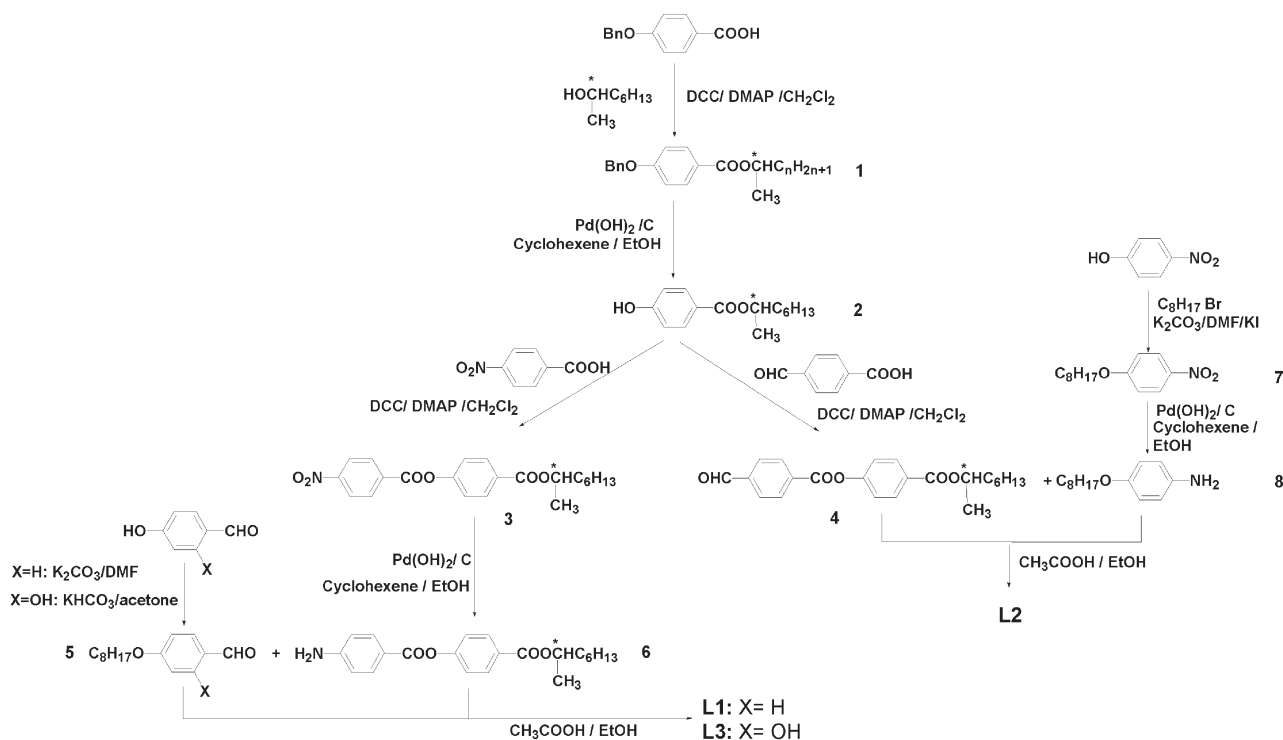


Chart 2



Results and discussion

Study of the ligands

Synthesis. The synthetic route used to prepare the ligands is shown in Scheme 1. The final step is, in all cases, the condensation of the aniline and the corresponding aldehyde to form the imine linkage.

The chiral tail, (2*R*)-2-octanol, was coupled with benzyl-protected 4-hydroxybenzoic acid using dicyclohexylcarbodiimide as esterification agent. The chiral phenol (**2**) was coupled either with *p*-nitrobenzoic acid (the nitro group was subsequently reduced to amino) or *p*-formylbenzoic acid to yield the corresponding chiral moieties (**3** and **4**) of the final ligands. These chiral moieties were coupled with the corresponding 4-alkoxybenzaldehyde (**5**) and *p*-alkoxyaniline (**8**) respectively, in ethanol with acetic acid as catalyst. These reactions gave the target Schiff bases.

Mesomorphic properties. The thermal properties of the ligands were investigated by polarising microscopy and differential scanning calorimetry. Results are given in Table 1.

All of the ligands prepared show mesomorphic behaviour

Table 1 Thermal properties of the ligands and their palladium complexes

Compound	Transition temperature/ ^o C [transition enthalpy, Δ <i>H</i> /kJ mol ⁻¹]
L1	Cr 110 [37.9] (SmC* _A 108 ^a) SmC* 125 [0.1] SmA 151[4.2] I
L2	Cr 74 [27.1] (SmI* _A 56 [1.9]) SmC* _A 114 [0.1] SmC* 123 [0.4] SmA 158 [4.7] I
L3	Cr 108 [32.5] SmC* _A 112 ^a SmC* 139 ^a SmA 173 [4.5] I
L1-PdAc	Cr 201 [37.9] SmA 205 dec
L1-PdCl	Cr 188 [37.3] (SmC* 185 ^a) SmA 240 dec
L2-PdAc	Cr 164 [4.7] SmA 196 dec
L2-PdCl	Cr 162 [23.3] SmC* _A 198 ^a SmA 250 dec
L3-Pd	Cr 225 [59.7] SmA 270 dec

^a Transition temperatures taken from optical microscopy observations.

over a wide temperature range (Table 1). Moreover, three of them show the potentially ferroelectric SmC* mesophase. The antiferroelectric mesophase was detected by both optical microscopy and DSC for compound **L2** but only by observation of textures through polarising optical microscopy for **L1** and **L3**. In all three ligands the SmC*_A mesophase was further confirmed by dielectric spectroscopy studies, as will be discussed below.

Two structural factors will be considered as far as their influence on the mesomorphic behaviour is concerned: (i) relative orientation of the dipoles along the long molecular axis; and (ii) presence of lateral polar groups such as a hydroxy group, which can affect the rigidity and polarisability of the mesogenic nucleus by means of intramolecular hydrogen bonding.

Comparison of the mesomorphic behaviour of compounds **L1** and **L2** shows that there is a significant effect when the orientation of dipoles along the molecular long axis is modified. Thus, dipoles in **L1** are all oriented head-to-tail whereas the sense of the imino linkage has been reversed in **L2**. One of the consequences of the inversion of this linking group is a marked decrease in the melting point without significantly affecting the clearing temperature. Furthermore, smectic polymorphism is significantly favoured; and an enantiotropic antiferroelectric SmC*_A is observed below the SmC* phase as well as an interval of coexistence of ferroelectric and antiferroelectric behaviour being deduced from dielectric spectroscopy and spontaneous polarisation studies. Below the antiferroelectric mesophase, a monotropic SmI*_A mesophase appears, and this behaves in an antiferroelectric manner under an electric field. The compound does not crystallize on cooling till room temperature but undergoes a cold crystallization during the subsequent heating process (see Fig. 2).

As a general trend, the mesomorphic interval increases when the rigidity of the mesogenic nucleus and its polarisability are enhanced by intramolecular hydrogen bonding. This situation is as one would expect for mesogenic molecules derived from salicylaldimines.⁸ Thus, compound **L3** shows a mesophase interval 24 °C wider than its analogue **L1**, which does not have the possibility of intramolecular H-bond. The melting temperatures are similar but the clearing point is 22 °C higher

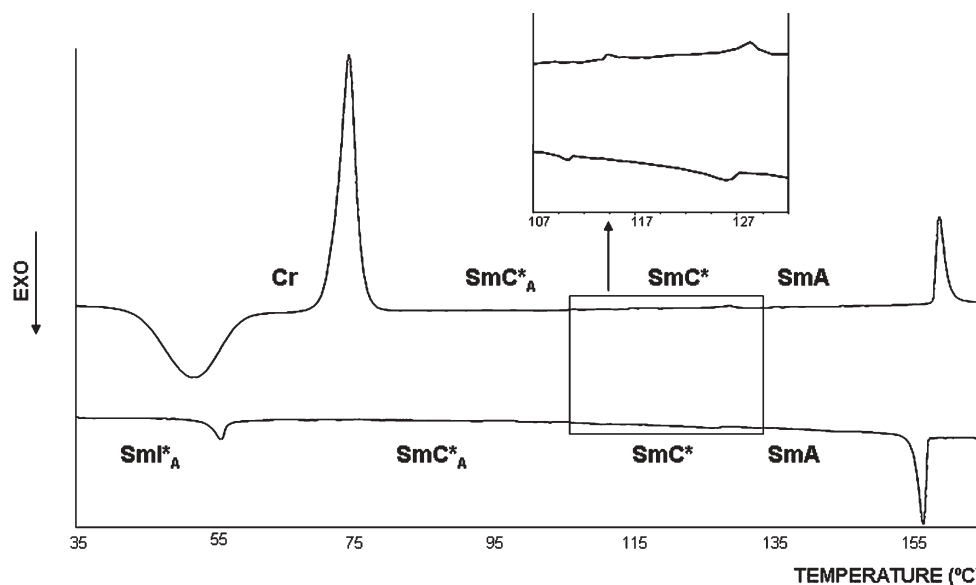


Fig. 2 DSC scans of compound **L2** during the second heating and cooling processes. Inset: expansion of the temperature interval in which transitions between SmA, SmC* and SmC*_A appear.

than that of **L1**. This extension of mesomorphic behaviour drastically affects the SmC* mesophase and gives rise to polymorphism. An enantiotropic antiferroelectric SmC*_A mesophase appears along with an interval of coexistence of ferroelectric and antiferroelectric behaviour (deduced from dielectric and spontaneous polarisation studies).

Texture analysis. Analysis of the textures allowed the identification of the type of smectic mesophase appearing in each compound. The change to antiferroelectric ordering in the tilted smectic mesophase in **L1**, **L2** and **L3** was particularly clear.

The natural texture of the SmA mesophase, on cooling from the isotropic state, is fan-shaped with black zones corresponding to homeotropic alignment of the molecules. Further cooling yields a broken fan-shaped texture corresponding to the tilted SmC* and this shows dechiralization lines at certain temperature intervals within the ferroelectric SmC* mesophase. In **L1** and **L2**, the pseudohomeotropic texture of the SmC* phase arising from the homeotropic alignment in the SmA mesophase appears red initially (Fig. 3a) and then turns green on cooling (Fig. 3b and 3c). At a given temperature the colour again becomes red (Fig. 3d), which signifies unwinding of the helix.⁹

This observation is in contrast to that occurring in the ferroelectric SmC* phase, whose helix becomes tighter as the temperature decreases. This phenomenon, which is clearly detectable, allowed confirmation of antiferroelectric ordering in these compounds. Moreover, at a temperature close to the transition to the antiferroelectric mesophase, both compounds show an iridescent petal texture due to a helix pitch in the visible region of the spectrum, with the visible light being blue-green. In the case of compounds **L2** and **L3**, the dechiralization lines visible in the ferroelectric SmC* mesophase disappear on reaching the antiferroelectric ordering. The SmI*_A mesophase of compound **L2** was identified by its bubble texture on cooling from the SmC*_A mesophase. Confirmation of this mesophase, as opposed to SmF*, came from the observation of its *Schlieren* texture (arising from the pseudohomeotropic zones of the SmC*_A), which was difficult to be focused. Dechiralization lines related to the helix of the phase reappear when this mesophase forms.

Ferroelectric properties of the ligands. All the three ligands were studied under the influence of an alternating electric field in 5 μm cells with polyimide coating (to achieve homogeneous alignment) and inner ITO electrodes. The spontaneous

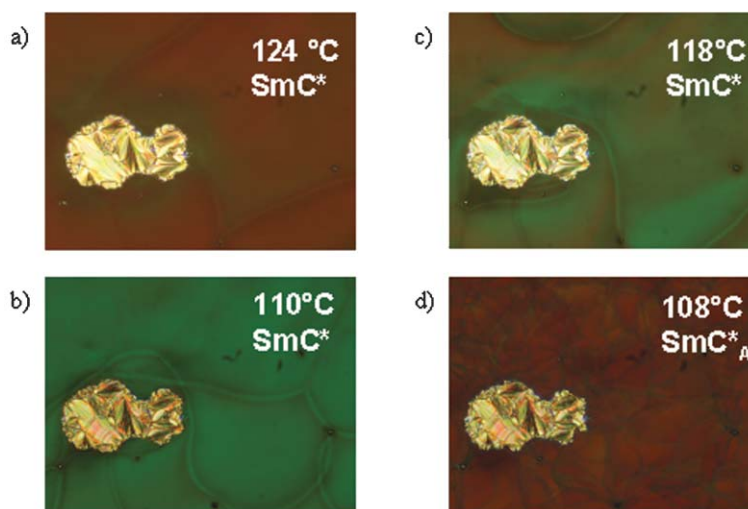


Fig. 3 Photomicrographs of **L2** in its SmC* and SmC*_A mesophases. The pseudohomeotropic texture of the SmC* appears red (a) and turns green on cooling (b and c). At the transition to the antiferroelectric mesophase, it becomes red again (d).

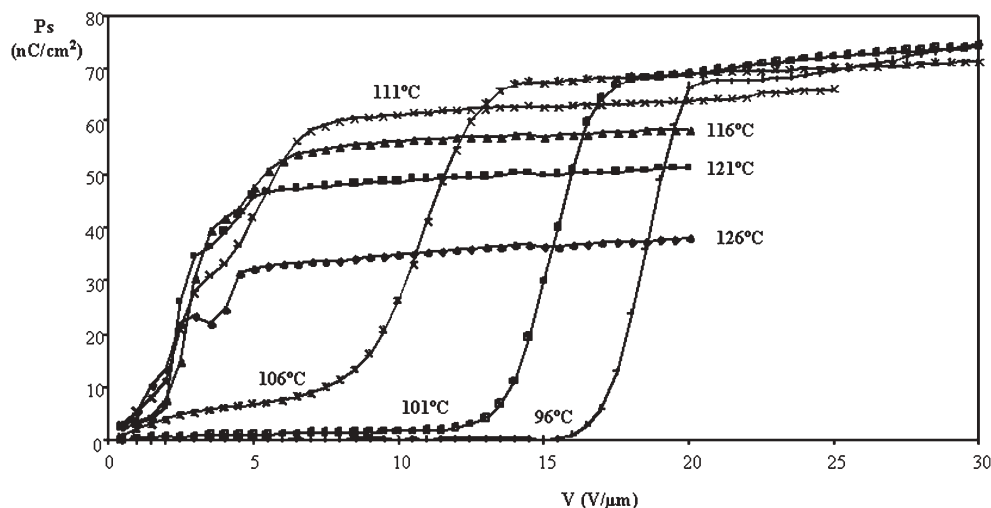


Fig. 4 Plot of the spontaneous polarisation values against the electric field at different temperatures for **L2**. Measurements were carried out in a 5 μm Linkam cell.

polarisation (P_s) was evaluated by means of the triangular wave method.¹⁰ The maximum value reached in all cases was around 80 nC cm^{-2} (85 nC cm^{-2} for compound **L1** and 80 nC cm^{-2} for **L2** and **L3**). The sign of the P_s was negative in all the three cases. Measurements were made at $8.5 V_{pp} \mu\text{m}^{-1}$ and 50 Hz (V_{pp} = voltage peak to peak). For **L2**, it was necessary to employ $20 V_{pp} \mu\text{m}^{-1}$ in order to induce ferroelectric switching over the whole range of ferro- and antiferroelectric mesophases. **L1** and **L3** show a dependence of the spontaneous polarisation values on the applied electric field as one would expect for a ferroelectric behaviour. **L2** was an exception to this trend. Fig. 4 shows the measured polarisation for different values of the maximum field of the triangular wave (50 Hz) for different temperatures, both in the SmC^* phase and in the SmC^*_A phase. For the last mesophase, although the switching current shows only a peak for each half period, the behaviour is clearly antiferroelectric with a very clear threshold field that increases as temperature decreases.¹¹

The formation of antiferroelectric order below the ferroelectric mesophase, which would be the responsible for the special textural appearance observed for **L1**, **L2** and **L3**, was confirmed by means of dielectric spectroscopy. Fig. 5 shows the dielectric permittivity at 125 Hz in a Linkam cell (5 μm) and at

1 kHz in a metallic cell (50 μm) for compound **L2**. Fig. 6 shows the corresponding results for compound **L3** at 125 Hz in a metallic cell (50 μm). All the samples were studied on cooling. The huge increase corresponds to the SmA – SmC^* phase transition and the step decrease to the SmC^* – SmC^*_A transition. For **L1** (not shown) the decrease coincides with the change in texture but the compound crystallizes immediately, making it impossible to perform any study in the antiferroelectric mesophase. For **L3** the SmC^*_A phase persists over several degrees but any attempt to measure the spontaneous polarisation during this period was unsuccessful because of field-induced crystallization. In Linkam cells the interval over which the antiferroelectric mesophase exists almost disappears. The temperature interval associated with the large value of the permittivity (for the three compounds) does not correspond to pure ferroelectric behaviour, probably due to the coexistence of ferro- and antiferroelectric behaviour. In Fig. 5 one can also see that for **L2** the transition from the ferroelectric to the antiferroelectric mesophase is sharper in the metallic cell than in the Linkam cell. Similar effects have also been observed by other authors.¹²

As far as the structural modifications influencing ferroelectric properties are concerned (*i.e.* P_s), significant effects

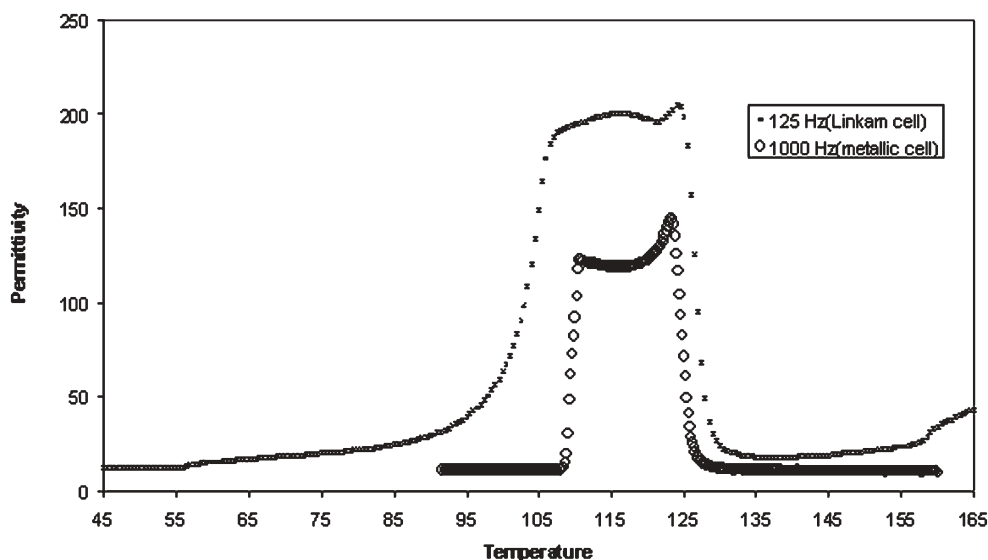


Fig. 5 Plots of the dielectric permittivity against temperature for compound **L2** measured at 125 Hz in a 5 μm Linkam cell and at 1 kHz in a 50 μm thick metallic cell on cooling.

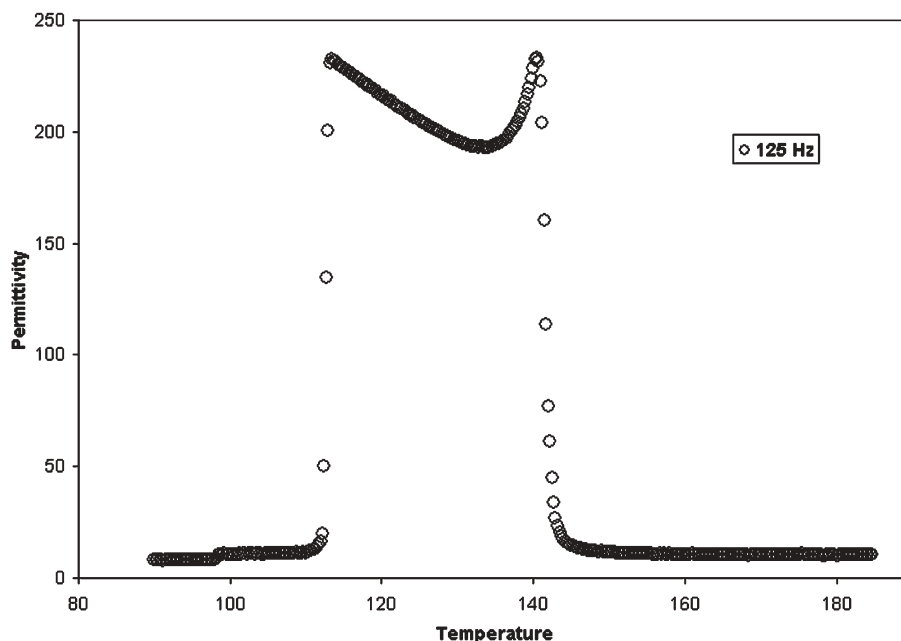


Fig. 6 Plot of the dielectric permittivity against temperature for compound L3 measured at 125 Hz in a 50 μm thick metallic cell on cooling.

were not detected compared to those observed for mesomorphic behaviour. Neither reversing dipoles along the molecular long axis nor having a lateral hydroxy group in the mesogenic core showed any influence on the P_s values, which are in all cases around 80 nC cm^{-2} .

Study of the complexes

The metal complexes were prepared by coordination of both benzaldimine ligands (L1 and L2) and the salicylaldimine ligand (L3) with palladium(II). The metal was coordinated to the corresponding ligands according to their nature. Thus, L1 and L2 give rise to dinuclear-*ortho*-palladated complexes, in which bridges between palladium atoms are either acetate or chlorine. On the other hand, ligand L3 gives rise to a *N,O*-chelated mononuclear palladium(II) complex. By means of both strategies, dimeric molecules have been built with an antiparallel orientation of their corresponding mesogenic chiral ligands.

Synthesis of the complexes. The preparation of the *ortho*-palladated complexes was carried out by reaction of the ligand with palladium(II) acetate in glacial acetic acid. Two acetate-bridged complexes, L1-PdAc and L2-PdAc, were obtained in this way. In both cases the *trans* isomer was only observed by $^1\text{H NMR}$ studies. The chloro-bridged complexes, L1-PdCl and L2-PdCl, were prepared from the corresponding acetate derivatives by reaction with HCl in methanol (see Scheme 2a). The presence of only one isomer, *i.e.* *trans*, was again indicated by $^1\text{H NMR}$ studies.

Mesomorphic behaviour. The transition temperatures and enthalpies corresponding to the complexes studied are gathered in Table 1.

Textures for *ortho*-palladated compounds were observed on cooling from the SmA mesophase as decomposition was detected at around 200°C . The SmA showed a homeotropic texture that turned into a *Schlieren*, pseudohomeotropic, texture corresponding to the SmC* phase for L1-PdCl. In the case of L2-PdCl the homeotropic SmA texture gave rise to a grey marbled appearance below the transition to the antiferroelectric SmC*_A mesophase. Similarly, usual fan-shaped and homeotropic textures were observed for the SmA mesophase of the salicylaldimine complex L3-Pd. However, this

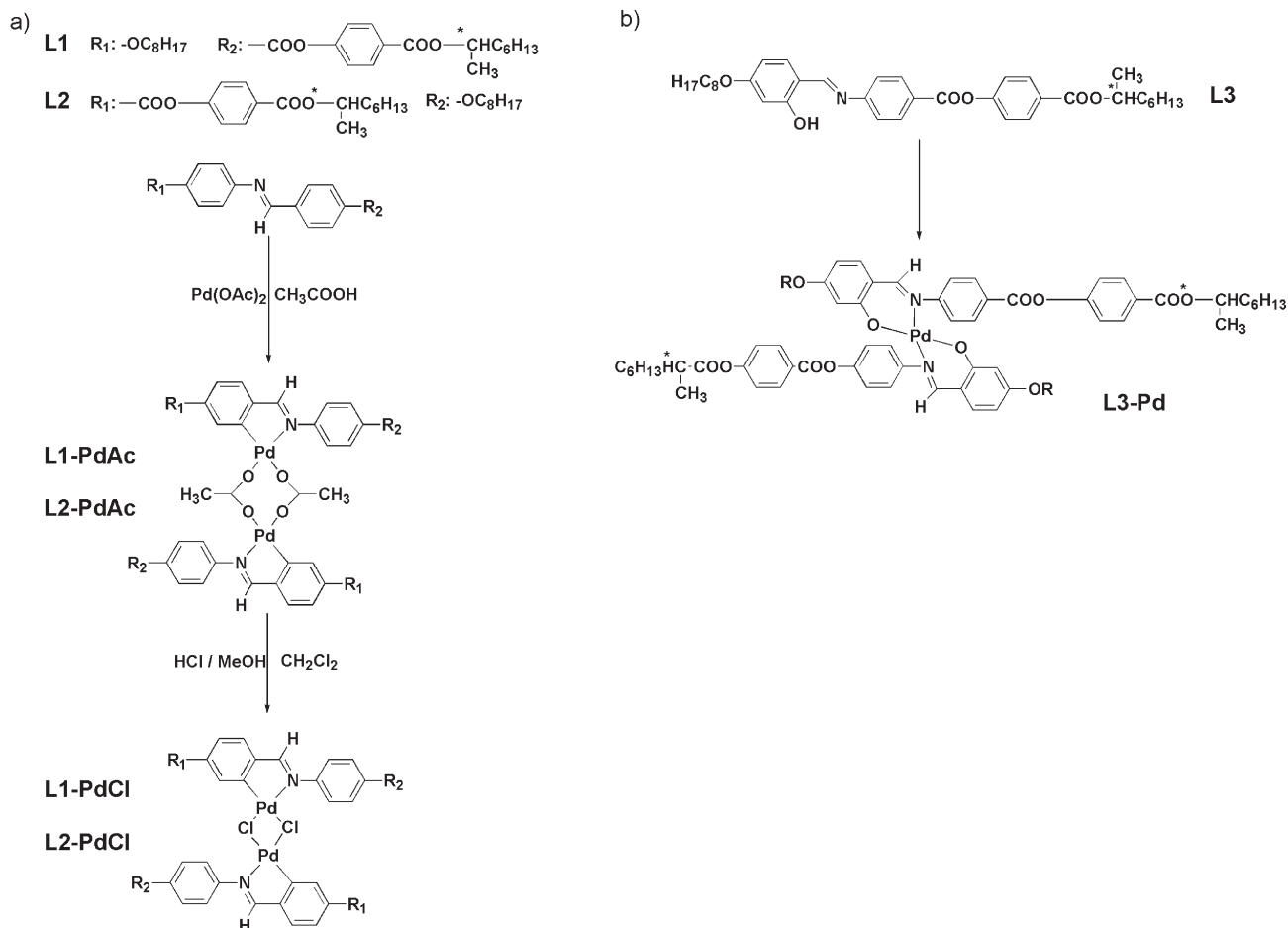
compound also showed decomposition on reaching the clearing temperature.

On the basis of all the experimental results, it can be seen that all the complexes organized themselves into the orthogonal SmA mesophase up to decomposition, irrespective of the planarity of their structures. However, the appearance of the tilted chiral SmC mesophases is basically observed for planar structures only. Furthermore, the targeted antiferroelectric SmC*_A order is exclusive for compound L2-PdCl and is seen over a range of 40°C , with complete absence of the ferroelectric SmC* mesophase.

Comparison of the types of mesophase and their temperature ranges of both the ligands and their related complexes (see Table 1) shows that, along with the expected increase of the transition temperatures and stabilization of the liquid crystal order for the complexes, no dramatic modifications of the mesophase range occur on going from the ligand to the complex. However, a significant change in the mesomorphic order is clear. For example, the orthogonal SmA is favoured for the metal-containing molecules, while the decrease or total suppression of tilted SmC* phases are apparent.

Ferroelectric properties of the complexes. Maximum spontaneous polarisation values were measured for the complexes displaying an enantiotropic SmC* phase, *i.e.* L3-Pd (36 nC cm^{-2} , measured under $10 \text{ Vpp } \mu\text{m}^{-1}$ and a frequency of 50 Hz), or the antiferroelectric SmC*_A mesophase, L2-PdCl (15 nC cm^{-2} , measured under $35 \text{ Vpp } \mu\text{m}^{-1}$ and a frequency of 50 Hz). During the study of the mesophase of L2-PdCl, even though only a single current peak was observed upon application of a triangular-wave electric field, a threshold voltage around $30 \text{ V } \mu\text{m}^{-1}$ was clearly detected. Such a result is indicative of the existence of antiferroelectric ordering within the mesophase. This phenomenon occurred over the whole range of the tilted mesophase. The dielectric studies also confirm the antiferroelectric nature of the tilted phase. Fig. 7 shows the dielectric permittivity at 1 kHz on cooling (the value measured almost corresponds to the static value because all the relaxations present occur at higher frequencies) and this shows typical soft mode behaviour. A mode that could be described as a ferroelectric Goldstone mode was not observed.

One of the targets of our work was the induction or stabilization of the antiferroelectric ordering upon dimerization



Scheme 2

through complexation. Although induction of this mesophase was not observed in any case, the appearance of antiferroelectric switching in a metallomesogen has been accomplished. Thus, the ligand **L2**, which shows SmC^* and SmC^*_A mesophases, gives rise to a chloro-bridged complex, **L2-PdCl**, that shows enantiotropic antiferroelectric behaviour over a range of 40 °C, up to 190 °C. This phase appears below the SmA phase, as confirmed by dielectric studies (P_s measurements and broadband dielectric spectroscopy). In fact, we can propose this type of dimerization as an approach for the design of antiferroelectric liquid crystals that ensures an antiparallel disposition of the linked monomers. This strategy can be

considered as an alternative to previously reported strategies based on twining calamitic molecules, either by terminally attached or laterally connected monomers, which have afforded antiferroelectric liquid crystalline materials.¹³

However, even though the restricted antiparallel arrangement of the chiral ligands has been ensured by means of metal coordination, *trans* complexation only maintains the highly polar character in the smectic layers of the ligands in one case, **L2-PdCl**. Thus, from ligands that show an enantiotropic antiferroelectric mesophase, *i.e.* **L3** and **L2**, only an antiferroelectric mesophase has been achieved for the dinuclear *ortho*-palladated complex **L2-PdCl**. In contrast, **L3-Pd** does not

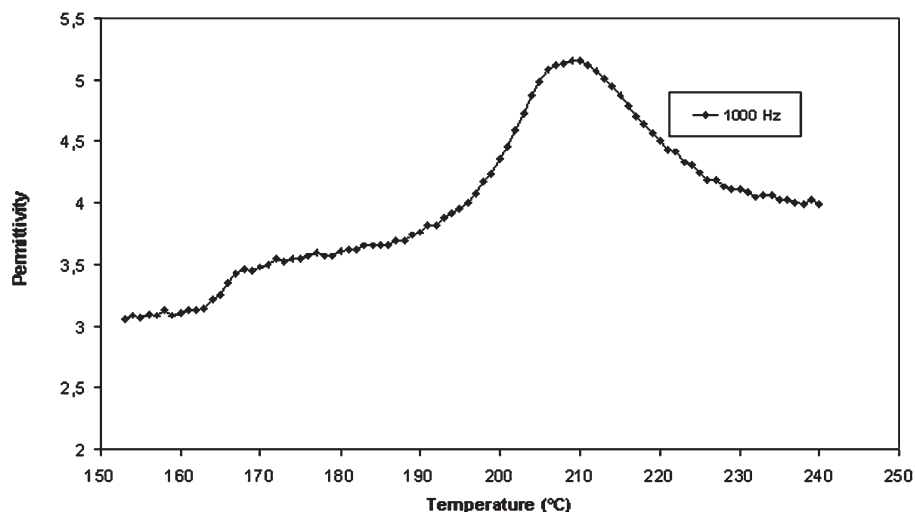


Fig. 7 Plot of the dielectric permittivity against temperature for complex **L2-PdCl** measured at 1 kHz in a 50 μm thick metallic cell on cooling.

maintain the antiferroelectric behaviour shown by the ligand itself. This is related to recent results of metal-complexation experiments of salicylaldehyde banana-shaped ligands, in which disappearance of the switchable B2 mesophase occurs for metal complexes prepared from ligands that show the mesophase in a wide temperature interval.¹⁴

Conclusion

We have described the synthesis and mesomorphic and dielectric characterization of a series of new imine-based liquid crystalline compounds that exhibit tilted SmC* phases. These compounds have offered the possibility of analysing and establishing the effect of different structural modifications on mesomorphism and dielectric behavior. In addition, these imines have allowed a new approach to the design of antiferroelectric liquid crystals to be investigated. The complexation of these ligands to palladium(II) gives rise to new ferroelectric materials. It is worth noting that transfer of the tendency to form antiferroelectric order from the ligand to the metal derivative has been accomplished for a chloro-bridged-*ortho*-palladated compound. This represents an alternative strategy to a more general approach to the design of antiferroelectric materials based on dimerization of chiral smectogenic molecules.

Experimental

Synthesis of (1*R*)-1-methylheptyl 4-benzyloxybenzoate (1)

To a solution of 15 mmol of (2*R*)-2-octanol in 150 mL of distilled dichloromethane were added 15 mmol of 4-benzyloxybenzoic acid and 1.5 mmol of dimethylaminopyridine (DMAP) under an argon atmosphere. The mixture was cooled in an ice/water bath and, after 10 min, 15 mmol of dicyclohexylcarbodiimide (DCC) were added under an argon atmosphere. The mixture was stirred overnight at room temperature, the salts were filtered off and the solvent was evaporated. The crude product was purified by flash chromatography using a mixture of hexanes/ethyl acetate (7:1) as eluent. Yield: 68% of a yellow oil. R_f : 0.72 (8:2 hexanes/ethyl acetate). $^1\text{H-RMN}$ (300 MHz, CDCl_3): δ 0.87 (t, $J = 7.0$ Hz, 3 H), 1.27 (m, 8 H), 1.31 (d, $J = 6.2$ Hz, 3 H), 1.57 (m, 1 H), 1.69 (m, 1 H), 5.1 (m, 3 H), 6.98 (d, $J = 8.9$ Hz, 2 H), 7.32–7.44 (m, 5 H), 7.99 (d, $J = 8.9$ Hz, 2 H). $^{13}\text{C-RMN}$ (300 MHz, CDCl_3): δ 14.1, 20.1, 22.6, 25.4, 29.2, 31.7, 36.1, 70.1, 71.4, 113.4, 123.6, 127.5, 128.2, 128.7, 131.5, 136.4, 162.3, 166.0. IR (Nujol) ν/cm^{-1} : 1708, 1276, 1251, 1167, 1105.

Synthesis of (1*R*)-1-methylheptyl 4-hydroxybenzoate (2)

To a mixture of 7.34 mmol of (1*R*)-1-methylheptyl 4-benzyloxybenzoate (1), were added 30 mL of cyclohexene and 60 mL of ethanol under an argon atmosphere. 0.5 g of $\text{Pd}(\text{OH})_2/\text{C}$ (20%) was then added in small portions. The mixture was refluxed for 24 h. The mixture was filtered through a pad of Celite[®] and the solvent was evaporated. The crude product was purified by flash chromatography using dichloromethane as eluent. Yield: 97% of a yellow oil. R_f : 0.43 (8:2 hexanes/ethyl acetate). $^1\text{H-RMN}$ (300 MHz, CDCl_3): δ 0.85 (t, $J = 7.1$ Hz, 3 H), 1.25 (m, 8 H), 1.30 (d, $J = 6.2$ Hz, 3 H), 1.59 (m, 1 H), 1.69 (m, 1 H), 5.1 (m, 1 H), 6.84 (d, $J = 8.9$ Hz, 2 H), 7.94 (d, $J = 8.9$ Hz, 2 H). $^{13}\text{C-RMN}$ (300 MHz, CDCl_3): δ 14.0, 20.0, 22.5, 25.3, 29.1, 31.7, 36.0, 72.1, 115.3, 122.2, 131.9, 160.9, 167.3. IR (Nujol) ν/cm^{-1} : 3351(w), 1709, 1678, 1284, 1231, 1166, 1115.

Synthesis of 4-[(1*R*)-1-methylheptyloxycarbonyl]phenyl 4-nitrobenzoate (3)

The esterification of *p*-nitrobenzoic acid with the corresponding phenol (2) was carried out with dicyclohexylcarbodiimide (DCC) and dimethylaminopyridine (DMAP) in dichloromethane, in a similar way to that described for (1*R*)-1-methylheptyl 4-benzyloxybenzoate (1). The reaction was carried out at room temperature. The crude product was purified by flash chromatography on silica gel using a mixture of hexanes/ethyl acetate (1:7) as eluent. Yield: 68% of a white solid. R_f : 0.61 (8:2 hexanes/ethyl acetate). Mp: 36 °C. $^1\text{H-RMN}$ (300 MHz, CDCl_3): δ 0.86 (t, $J = 6.6$ Hz, 3 H), 1.27 (m, 8 H), 1.33 (d, $J = 6.3$ Hz, 3 H), 1.60 (m, 1 H), 1.71 (m, 1 H), 5.15 (m, 1 H), 7.30 (d, $J = 8.7$ Hz, 2 H), 8.13 (d, $J = 8.7$ Hz, 2 H), 8.37 (s, 4 H). $^{13}\text{C-RMN}$ (300 MHz, CDCl_3): δ 14.0, 20.0, 22.6, 25.4, 29.1, 31.7, 36.0, 72.1, 121.4, 123.8, 129.1, 131.2, 131.3, 134.5, 150.9, 153.8, 162.8, 165.2. IR (Nujol) ν/cm^{-1} : 1746, 1712, 1528, 1349, 1261, 1201, 1162, 1110.

Synthesis of 4-[(1*R*)-1-methylheptyloxycarbonyl]phenyl 4-formylbenzoate (4)

The esterification of *p*-formylbenzoic acid with the corresponding phenol (2) was carried out with dicyclohexylcarbodiimide (DCC) and dimethylaminopyridine (DMAP) in dichloromethane, in a similar way to that described for (3). The crude product was purified by flash chromatography using a mixture of hexanes/ethyl acetate (9:1) as eluent. Yield: 69%. R_f : 0.54 (8:2 hexanes/ethyl acetate). $^1\text{H-RMN}$ (300 MHz, CDCl_3): δ 0.86 (m, 3 H), 1.26 (m, 8 H), 1.33 (d, $J = 6.2$ Hz, 3 H), 1.59 (m, 1 H), 1.71 (m, 1 H), 5.15 (m, 1 H), 7.27 (d, $J = 8.7$ Hz, 2 H), 8.02 (d, $J = 8.4$ Hz, 2 H), 8.12 (d, $J = 8.7$ Hz, 2 H), 8.35 (d, $J = 8.4$ Hz, 2 H), 10.13 (s, 1 H). $^{13}\text{C-RMN}$ (300 MHz, CDCl_3): δ 14.1, 20.1, 22.6, 25.4, 29.2, 31.8, 36.1, 72.1, 121.5, 129.0, 129.7, 130.9, 131.3, 134.1, 139.7, 154.1, 163.7, 165.3, 191.5. IR (Nujol) ν/cm^{-1} : 2856, 1746, 1712, 1260, 1199.

Synthesis of 4-octyloxy-2-hydroxybenzaldehyde (5, X = OH)

A mixture of 14 mmol of 2,4-dihydroxybenzaldehyde, 14 mmol of *n*-octyl bromide and 14 mmol of dry potassium bicarbonate in 60 mL of dry acetone was refluxed for 90 h under an argon atmosphere. The reaction advanced slowly and was checked by TLC. The reaction was stopped when the TLC plate showed that the diether compound began to appear. The mixture was filtered through a pad of Celite[®] to remove the inorganic salts and the solvent was evaporated. The crude product was purified by flash chromatography using a mixture of hexanes/ethyl acetate (3:1) as eluent. Yield: 54% of an orange oil. R_f : 0.76 (8:2 hexanes/ethyl acetate). $^1\text{H-RMN}$ (300 MHz, CDCl_3): δ 0.88 (t, $J = 6.2$ Hz, 3 H), 1.2–1.5 (m, 10 H) 1.81 (t, $J = 6.6$ Hz, 2 H), 6.38 (d, $J = 2.2$ Hz, 1 H) 6.5 (dd, $J = 2.2$ Hz, $J = 8.8$ Hz, 1 H), 7.37 (d, $J = 8.8$ Hz, 1 H) 9.69 (s, 1 H). IR (Nujol) ν/cm^{-1} : 3037 (w), 1643, 1630, 1221.

Synthesis of 4-octyloxybenzaldehyde (5, X = H)

A mixture of 34 mmol of 4-hydroxybenzaldehyde, 34 mmol of *n*-octyl bromide and 34 mmol of potassium carbonate in 30 mL of dimethylformamide was heated at 80 °C under an argon atmosphere for 8 h. The mixture was poured into 60 mL of water and then the aqueous layer was extracted several times with a mixture of hexanes/ethyl acetate (1:1), the combined organic layers were extracted with 2 M sodium hydroxide, washed with brine, water, dried over magnesium sulfate and then the solvent was evaporated. The compound was purified by flash chromatography using a mixture of hexanes/ethyl acetate (4:1) as eluent. Yield: 48% of yellowish oil. R_f : 0.68 (8:2 hexanes/ethyl acetate). $^1\text{H-RMN}$ (300 MHz, CDCl_3): δ 0.86 (t, $J = 6.9$ Hz, 3 H), 1.26–1.46 (m, 10 H) 1.79 (m, 2 H), 4.01 (t,

$J = 6.6$ Hz, 2 H), 6.97 (d, $J = 8.8$ Hz, 2 H), 7.78 (d, $J = 8.6$ Hz, 1 H), 9.85 (s, 1 H). IR (Nujol): ν/cm^{-1} : 2733, 1690, 1601, 1259, 1159, 1140.

Synthesis of 4-(1-methylheptyloxycarbonyl)phenyl 4-aminobenzoate (6)

To 1 mmol of **3** (obtained as described the previous steps) in 16 mL of a mixture cyclohexene/absolute ethanol (1:1), was added 68 mg of Pd(OH)₂/C in small portions under an argon atmosphere. The suspension was refluxed for 90 min. The mixture was cooled down, filtered through a pad of Celite[®], and the crude product was used in the next reaction without further purification. The pure compound was obtained by recrystallization from ethanol/water (3:1). Yield: 98% of a white solid. R_f : 0.17 (8:2 hexanes/ethyl acetate). Mp: 77 °C. ¹H-RMN (300 MHz, CDCl₃): δ 0.85 (t, $J = 7.1$ Hz, 3 H), 1.26 (m, 8 H), 1.32 (t, $J = 6.2$ Hz, 2 H), 1.59 (m, 1 H), 1.66 (m, 1 H), 4.16 (s, 2 H), 5.13 (m, 1 H), 6.67 (d, $J = 8.8$ Hz, 2 H), 7.24 (d, $J = 8.8$ Hz, 2 H), 7.98 (d, $J = 8.8$ Hz, 2 H), 8.08 (d, $J = 8.8$ Hz, 2 H). ¹³C-RMN (300 MHz, CDCl₃): δ 14.1, 20.1, 22.6, 25.4, 29.1, 31.7, 36.1, 71.9, 113.8, 118.1, 121.8, 128.1, 131.0, 132.5, 151.8, 154.9, 164.7, 165.6. IR (Nujol) ν/cm^{-1} : 3460, 3362, 3224, 1703, 1279, 1205, 1171, 1064.

Synthesis of 4-octyloxynitrobenzene (7)

The compound was synthesized using the same synthetic method as described for 4-octyloxybenzaldehyde (**5**), and was used in the next step without further purification. Yield: 70%. R_f : 0.75 (8:2 hexanes/ethyl acetate). ¹H-RMN (300 MHz, CDCl₃): δ 0.86 (m, 3 H), 1.27–1.55 (m, 10 H), 1.75–1.82 (m, 2 H), 4.02 (t, $J = 6$ Hz, 2 H), 6.91 (d, $J = 9$ Hz, 2 H), 8.16 (d, $J = 9$ Hz, 2 H).

Synthesis of 4-octyloxyaniline (8)

The compound was synthesized using the same synthetic method as that described for compound **6**. The product was used in the next step without further purification.

Yield: 98%. ¹H-RMN (300 MHz, CDCl₃): δ 0.87 (m, 3 H), 1.22–1.41 (m, 8 H), 1.69–1.74 (m, 4 H), 3.12 (s, 2 H), 3.85 (t, $J = 9$ Hz, 2 H), 6.61 (d, $J = 9$ Hz, 2 H), 6.72 (d, $J = 9$ Hz, 2 H). IR (Nujol) ν/cm^{-1} : 3408, 3315, 3221, 2952, 1631, 1511, 1233.

Synthesis of 4-[(1R)-1-methylheptyloxycarbonyl]phenyl N-(4'-octyloxybenzylidene)-4-aminobenzoate, L1

A mixture of 1 mmol of 4-octyloxybenzaldehyde (**5**, X = H) and 1 mmol of 4-(1-methylheptyloxycarbonyl)phenyl 4-aminobenzoate (**6**) and 5 drops of acetic acid in 20 mL of absolute ethanol was stirred for 4 h at room temperature under an argon atmosphere. The solid was collected and recrystallized from technical ethanol. Yield: 60% of a white solid. ¹H-RMN (300 MHz, CDCl₃): δ 0.87 (m, 6 H), 1.28–1.33 (m, 21 H), 1.54–1.60 (m, 1 H), 1.70–1.82 (m, 3 H), 4.02 (t, $J = 6.3$ Hz, 2 H), 5.15 (m, 1 H), 6.97 (d, $J = 8.4$ Hz, 2 H), 7.24 (d, $J = 8.7$ Hz, 2 H), 7.29 (d, $J = 8.7$ Hz, 2 H), 7.84 (d, $J = 8.4$ Hz, 2 H), 8.11 (d, $J = 8.7$ Hz, 2 H), 8.20 (d, $J = 8.7$ Hz, 2 H), 8.36 (s, 1 H). ¹³C-RMN (300 MHz, CDCl₃): δ 14.0, 14.1, 20.1, 22.5, 22.6, 25.4, 25.9, 29.1, 29.2, 29.3, 31.7, 31.8, 36.0, 68.3, 71.9, 114.8, 121.0, 121.7, 125.7, 128.5, 130.9, 131.1, 131.6, 154.5, 157.3, 161.2, 162.2, 162.4, 164.5, 165.5. IR (Nujol) ν/cm^{-1} : 1733, 1712, 1621, 1593, 1573, 1277. Anal. Calc. for C₃₇H₄₇NO₅: C 75.86, H 8.09, N 2.39; Found: C 75.82; H 8.12; N 2.49%. MS (FAB+) m/z : (M + 1) 586, 474, 360, 336 (100%).

Synthesis of N-{4'-[4''-(1R)-1-methylheptyloxycarbonyl]-phenoxybenzylidene}-4-octyloxyaniline, L2

The compound was synthesized from **4** and **8** using the same synthetic method as described for compound **L1**. Yield: 63% of a yellowish solid. ¹H-RMN (300 MHz, CDCl₃): δ 0.86 (s, 6 H), 1.27–1.34 (m, 21 H), 1.46–1.53 (m, 1 H), 1.74–1.80 (m, 3 H), 3.97 (t, $J = 6.9$ Hz, 2 H), 5.11 (m, 1 H), 6.93 (d, $J = 8.7$ Hz, 2 H), 7.28 (m, 4 H), 8.02 (d, $J = 8.1$ Hz, 2 H), 8.12 (d, $J = 8.7$ Hz, 2 H), 8.27 (d, $J = 8.1$ Hz, 2 H), 8.57 (s, 1 H). ¹³C-RMN (300 MHz, CDCl₃): δ 14.1, 20.1, 22.6, 22.7, 25.4, 26.0, 29.1, 29.2, 29.4, 30.9, 31.7, 31.8, 36.1, 68.3, 72.0, 115.1, 121.6, 122.5, 128.5, 128.7, 130.6, 130.8, 131.7, 141.2, 143.8, 154.3, 156.2, 158.5, 164.2, 165.4. IR (Nujol) ν/cm^{-1} : 1733, 1716, 1255. Anal. Calc. for C₃₇H₄₇NO₅: C 75.86, H 8.09, N 2.39; Found: C 75.84, H 8.14, N 2.43%. MS (FAB+) m/z : (M + 1) 586, 472, 336 (100%).

Synthesis of 4-[(1R)-1-methylheptyloxycarbonyl]phenyl N-(4'-octyloxy-2'-hydroxybenzylidene)-4-aminobenzoate, L3

A mixture of 1 mmol 4-octyloxy-2-hydroxybenzaldehyde (**5**, X = OH) and 1 mmol of 4-(1-methylheptyloxycarbonyl)phenyl 4-aminobenzoate (**6**) and 5 drops of acetic acid in 10 mL of absolute ethanol was refluxed for 4 h, cooled down and then stirred at room temperature overnight. The solid was collected and recrystallized from technical ethanol. Yield 45% of a yellow solid. ¹H-RMN (300 MHz, CDCl₃): δ 0.86 (m, 6 H), 1.23–1.45 (m, 21 H), 1.56–1.66 (m, 1 H), 1.66–1.84 (m, 3 H), 3.99 (t, $J = 6.6$ Hz, 2 H), 5.16 (m, 1 H), 6.50 (m, 2 H), 7.20–7.38 (m, 5 H), 8.1 (d, $J = 8.7$ Hz, 2 H), 8.22 (d, $J = 8.4$ Hz, 2 H), 8.55 (s, 1 H), 13.3 (s, 1 H). ¹³C-RMN (300 MHz, CDCl₃): δ 14.0, 20.0, 22.6, 25.4, 25.9, 29.00, 29.2, 29.3, 29.4, 29.6, 31.7, 36.0, 68.3, 71.9, 101.5, 108.1, 112.7, 121.2, 121.6, 126.5, 128.5, 131.1, 131.7, 134.0, 153.4, 154.4, 163.1, 164.1, 164.2, 164.3, 165.4. IR (Nujol) ν/cm^{-1} : 3433 (w), 1728, 1714, 1627, 1272, 1210, 1195. Anal. Calc. for C₃₇H₄₇NO₆: C 73.87, H 7.8, N 2.32; Found: C 73.87, H 7.8, N 2.27%. MS (FAB+) m/z : (M + 1) 602, 490, 352 (100%).

Preparation of the acetato-bridged complexes. General procedure

The palladium complexes were prepared from the metal salt palladium(II) acetate. The metal salt (236 mg, 1 mmol) was added to a solution of the ligand (600 mg, 1 mmol) in acetic acid (30 mL). The reaction mixture was stirred at 40 °C for 8 h and then cooled. The precipitate was filtered off and dissolved in dichloromethane. The resulting solution was filtered on Celite[®] and the complex was re-precipitated by addition of acetone.

Analytical data. L1-PdAc. Yield 30%. ¹H-RMN (300 MHz, CDCl₃): δ 0.85 (m, 12 H), 1.19–1.34 (m, 42 H), 1.58–1.75 (m, 8 H), 1.93 (s, 6 H), 3.48 (m, 2 H), 3.74 (m, 2 H), 5.15 (m, 2 H), 5.97 (d, $J = 2.1$, Hz, 2 H), 6.60 (dd, $J = 2.1$ Hz, $J = 8.7$ Hz, 2 H), 6.87 (d, $J = 8.7$ Hz, 2 H), 7.23 (d, $J = 8.4$ Hz, 4 H), 7.30 (d, $J = 8.7$ Hz, 4 H), 7.64 (s, 2 H), 7.93 (d, $J = 8.4$ Hz, 4 H), 8.11 (d, $J = 8.7$ Hz, 4 H). ¹³C-RMN (300 MHz, CDCl₃): δ 14.1, 20.1, 22.5, 22.6, 24.4, 25.4, 25.9, 29.1, 29.2, 29.3, 31.7, 31.8, 36.1, 68.0, 72.0, 111.7, 117.0, 121.5, 123.2, 127.0, 128.6, 129.9, 130.0, 130.1, 131.1, 137.8, 152.1, 154.3, 159.1, 160.7, 163.9, 165.4, 172.1, 180.4. IR (Nujol) ν/cm^{-1} : 1727, 1586, 1573, 1531. Anal. Calc. for (C₃₉H₄₉NO₇Pd)₂: C 62.44, H 6.58, N 1.87; Found: C 62.39, H 6.20, N 2.09%. MS (FAB+) m/z : (M) 1444, 788, 576, 472 (100%).

L2-PdAc. Yield 28%. ¹H-RMN (300 MHz, CDCl₃): δ 0.86 (m, 12 H), 1.28–1.34 (m, 42 H), 1.39–1.60 (M, 8 H), 1.96 (s, 6 H), 3.68 (t, $J = 6$ Hz, 4 H), 5.15 (m, 2 H), 6.60 (d, $J = 9$ Hz, 4 H), 6.71 (d, $J = 9$ Hz, 4 H), 7.31 (m, 8 H), 7.69 (s, 2 H), 7.85

(d, $J = 9$ Hz, 2 H), 8.10 (d, $J = 9$ Hz, 4 H). ^{13}C -RMN (300 MHz, CDCl_3): δ 14.0, 14.1, 20.1, 22.6, 22.7, 24.3, 25.4, 25.8, 29.1, 29.2, 29.3, 31.7, 31.8, 36.1, 68.2, 71.9, 113.6, 121.5, 123.9, 126.1, 126.6, 128.4, 129.0, 131.0, 133.2, 140.4, 149.9, 154.3, 154.4, 159.2, 164.1, 165.4, 170.0, 180.7. Anal. Calc. for $(\text{C}_{39}\text{H}_{49}\text{NO}_7\text{Pd})_2$: C 62.44, H 6.58, N 1.87; Found: C 62.50, H 6.17, N 2.05%. MS (FAB+) m/z : (M) 1444, 586, 472, 336 (100%).

Preparation of the chloro-bridged complexes. General procedure

The complexes with chloro bridges were prepared from the corresponding acetate-bridged derivatives. A 0.61 N solution of hydrochloric acid in methanol (0.17 mmol) was added to a solution of the acetate-bridged complex (0.084 mmol) in dichloromethane (4 mL). The reaction mixture was stirred at room temperature for 1 h. The solvent was removed under reduced pressure and the crude product was purified by flash chromatography on silica gel eluting with dichloromethane. The product was re-precipitated by adding acetone to a concentrated solution of the product in dichloromethane.

Analytical data. **L1-PdCl.** Yield 60%. ^1H -RMN (300 MHz, CDCl_3): δ 0.85 (m, 12 H), 1.19–1.34 (m, 42 H), 1.53–1.72 (m, 8 H), 3.93–3.98 (m, 4 H), 5.12–5.16 (m, 2 H), 6.59 (d, $J = 7.5$ Hz, 2 H), 6.78 (d, $J = 2.1$ Hz, 2 H), 7.25 (d, $J = 8.4$ Hz, 4 H), 7.38 (d, $J = 8.4$ Hz, 4 H), 7.5 (dd, $J = 2.1$ Hz, $J = 7.5$ Hz, 4 H), 7.90 (s, 2 H), 8.12 (d, $J = 8.4$ Hz, 4 H), 8.24 (d, $J = 7.5$ Hz, 4 H). ^{13}C -RMN (300 MHz, CDCl_3): δ 14.1, 20.1, 22.6, 25.4, 25.9, 29.0, 29.2, 29.3, 31.7, 31.8, 36.1, 68.3, 71.9, 111.5, 119.6, 121.6, 123.6, 128.0, 128.6, 130.7, 131.1, 138.3, 153.0, 154.4, 156.7, 160.8, 163.9, 165.4, 173.9. IR (Nujol) ν/cm^{-1} : 1733, 1712, 1621, 1593, 1573, 1277. Anal. Calc. for $(\text{C}_{37}\text{H}_{46}\text{NO}_5\text{PdCl})_2$: C 61.16, H 6.38, N 1.93; Found: C 61.26, H 6.20, N 2.09%. MS (FAB+) m/z : 586, 474, 360, 336 (100%).

L2-PdCl. Yield 48%. ^1H -RMN (300 MHz, CDCl_3): δ 0.87 (m, 12 H), 1.23–1.34 (m, 42 H), 1.55–1.70 (m, 8 H), 3.81 (t, $J = 5.7$ Hz, 4 H), 5.13 (m, 2 H), 6.85 (d, $J = 8.1$ Hz, 4 H), 7.24–7.27 (m, 8 H), 7.34 (d, $J = 7.5$ Hz, 2 H), 7.39 (d, $J = 8.1$ Hz, 2 H), 7.87 (d, $J = 7.5$ Hz, 2 H), 7.99 (s, 2 H), 8.09 (d, $J = 8.1$ Hz, 4 H). ^{13}C -RMN (300 MHz, CDCl_3): δ 14.0, 14.1, 20.1, 22.5, 22.6, 25.4, 26.0, 29.1, 29.2, 29.3, 31.7, 31.8, 36.1, 68.3, 71.9, 114.5, 121.6, 124.4, 127.0, 127.5, 128.5, 129.3, 131.1, 134.3, 141.2, 150.7, 152.9, 154.5, 157.5, 159.5, 164.0, 165.4, 172.3. IR (Nujol) ν/cm^{-1} : 1739, 1716, 1268. Anal. Calc. for $(\text{C}_{37}\text{H}_{46}\text{NO}_5\text{PdCl})_2$: C 61.16, H 6.38, N 1.93; Found: C 61.05, H 6.28, N 1.99%. MS (FAB+) m/z : (M - Cl) 1417, 586, 472, 336 (100%).

Preparation of L3-Pd

To a solution of 500 mg (0.83 mmol) of the imine ligand, **L3**, in 40 mL of absolute ethanol, a suspension of 93 mg (0.41 mmol) of palladium(II) acetate in ethanol was added dropwise. The reaction mixture was refluxed for 2 h, and then stirred at room temperature for 8 h. The precipitate was filtered off and dissolved in dichloromethane. The resulting solution was filtered on Celite[®] and the complex was precipitated by pouring the solution into cold ethanol. Yield 62%.

^1H -RMN (300 MHz, CDCl_3): δ 0.84 (m, 12 H), 1.22–1.34 (m, 42 H), 1.55–1.70 (m, 8 H), 3.77 (t, $J = 6.6$ Hz, 4 H), 5.15 (m, 2 H), 5.52 (d, $J = 2.1$ Hz, 2 H), 6.18 (dd, $J = 9$ Hz, $J = 2.1$ Hz, 2 H), 7.06 (d, $J = 9$ Hz, 2 H), 7.29 (d, $J = 8.7$ Hz, 4 H), 7.47 (d, $J = 8.7$ Hz, 4 H), 7.58 (s, 2 H), 8.12 (d, $J = 8.7$ Hz, 4 H), 8.25 (d, $J = 8.7$ Hz, 4 H). ^{13}C -RMN (300 MHz, CDCl_3): δ 14.0, 20.1, 22.5, 22.6, 25.4, 25.9, 28.9, 29.1, 29.3, 31.7, 31.8, 36.1, 38.1, 67.8, 71.9, 102.1, 107.3, 114.5, 121.6, 125.4, 127.0, 128.5, 130.4, 131.1, 135.8, 154.4, 154.5, 161.0, 164.2, 165.4, 165.7,

167.1. IR (Nujol) ν/cm^{-1} : 1727, 1713, 1266. Anal. Calc. for $(\text{C}_{37}\text{H}_{46}\text{NO}_6\text{Pd})_2$: C 67.9, H 7.0, N 2.15; Found: C 67.55, H 6.20, N 2.14%. MS (FAB+) m/z : (M) 1306, 602, 352 (100%).

Techniques

Infrared spectra for all the complexes were obtained by using a Perkin-Elmer 1600 (FTIR) spectrophotometer in the 400–4000 cm^{-1} spectral range. NMR spectra were recorded on a Bruker ARX 300 spectrometer in CDCl_3 solutions. Microanalysis was performed with a Perkin-Elmer 240 B microanalyser.

The textures of the mesophases were studied using an optical microscope (Olympus) with crossed polarisers and connected to a Linkam THMS 600 hot stage and a Linkam TMS 91 central processor. Microphotographs were taken with a DP12 Olympus camera, adapted to the microscope. Measurements of the transition temperatures were made using a TA2910 differential scanning calorimeter with a heating or cooling rate of 10 $^\circ\text{C min}^{-1}$. The apparatus was calibrated with indium (156.6 $^\circ\text{C}$, 28.44 J g^{-1}).

The complex permittivity was measured over 11 decades of frequency (10^{-2} to 10^9 Hz) using three different measuring systems: a Schulmberger 1260 frequency response analyser fitted with a high-impedance preamplifier of a variable gain (10^{-2} to 10^6 Hz), and two impedance analysers, the HP 4191A (10^2 to 10^7 Hz) and the HP 4192A (10^6 – 10^9 Hz).

The spontaneous polarisation was measured using the triangular wave method. In the experimental set-up the triangular wave voltage was supplied by a HP3245A Function Generator. The current–voltage cycles were recorded by a digital acquisition system, tech ADC488/16A. All equipment was interfaced to a computer.

Acknowledgements

This work was supported by the C.I.C.Y.T. (MAT 2000-1293-CO2).

References

- 1 K. Miyachi and A. Fukuda, in *Handbook of Liquid Crystals*, D. Demus, J. W. Goodby, G. W. Gray, H.-W. Spiess and V. Vill, ed., Wiley-VCH, Weinheim, 1998, vol. 2B, pp. 665–691; S. T. Lagerwall, *Ferroelectric and Antiferroelectric Liquid Crystals*, Wiley-VCH, Weinheim, 1999.
- 2 A. D. L. Chandani, E. Gorecka, Y. Ouchi, H. Takezoe and A. Fukuda, *Jpn. J. Appl. Phys.*, 1989, **29**, L1265–L1268.
- 3 Y. Suzuki, O. Nonaka, Y. Koide, N. Okabe, T. Hagiwara, I. Kawamura, N. Yamamoto, Y. Yamada and T. Kitazume, *Ferroelectrics*, 1993, **147**, 109–119.
- 4 (a) K. Hori and K. Endo, *Bull. Chem. Soc. Jpn.*, 1993, **66**, 46–50; (b) H. Hori, Y. Yamahara and K. Ito, *Ferroelectrics*, 1993, **147**, 91–94; (c) K. Okuyama, N. Kawamano, S. Uehori, K. Noguchi, N. Okabe, Y. Suzuki and I. Kawamura, *Mol. Cryst. Liq. Cryst.*, 1996, **276**, 193–201; (d) K. Hori and S. Kawamura, *Liq. Cryst.*, 1996, **20**, 311–319; (e) H. Allouchi, H.-T. Nguyen and M. Cotrait, *Mol. Cryst. Liq. Cryst.*, 1999, **328**, 375–382.
- 5 M. Marcos, J. L. Serrano, T. Sierra and M. J. Giménez, *Angew. Chem., Int. Ed. Engl.*, 1992, **31**, 1471–1472; M. Marcos, J. L. Serrano, T. Sierra and M. J. Giménez, *Chem. Mater.*, 1993, **5**, 1332–1337; M. J. Baena, J. Barberá, P. Espinet, A. Ezcurra, M. B. Ros and J. L. Serrano, *J. Am. Chem. Soc.*, 1994, **116**, 1065; R. Iglesias, M. Marcos, J. L. Serrano, T. Sierra and M. A. Pérez-Jubindo, *Chem. Mater.*, 1996, **8**, 2611–2617; For studies concerning achiral Schiff base complexes, see: J. L. Serrano and T. Sierra, in *Metallomesogens. Synthesis, Properties and Applications*, Wiley-VCH, Weinheim, 1996, ch. 3.
- 6 G. Heppke, P. Kleinberg and D. Löttsch, *Liq. Cryst.*, 1993, **14**, 67–71.
- 7 P. Espinet, E. Lalinde, M. Marcos, J. Pérez and J. L. Serrano, *Organometallics*, 1990, **9**, 555–560; J. Barberá, P. Espinet, E. Lalinde, M. Marcos and J. L. Serrano, *Liq. Cryst.*, 1987, **2**, 833–842; M. Lehmann, M. Marcos, J. L. Serrano, T. Sierra, C. Bolm, K. Weickhardt, A. Magnus and G. Moll, *Chem. Mater.*, 2001, **13**, 4374–4381.

- 8 J. Barberá, E. Meléndez, J. L. Serrano, T. Sierra, A. Ezcurra and M. A. Pérez-Jubindo, *Mol. Cryst. Liq. Cryst.*, 1989, **170**, 151–157; T. Sierra, E. Meléndez, J. L. Serrano, A. Ezcurra and M. A. Pérez-Jubindo, *Chem. Mater.*, 1991, **3**, 157–163.
- 9 J. W. Goodby, J. S. Patel and E. Chin, *J. Mater. Chem.*, 1992, **2**, 197–207.
- 10 M. A. Pérez-Jubindo, M. J. Tello and J. Fernández, *J. Phys. D*, 1981, **14**, 2305–2308.
- 11 S. Merino, M. R. de la Fuente, Y. González, M. A. Pérez Jubindo, B. Ros and J. A. Puértolas, *Phys. Rev. E*, 1996, **54**, 5169–5177; M. C. Artal, B. Ros, J. L. Serrano, M. R. de la Fuente and M. A. Pérez Jubindo, *Chem. Mater.*, 2001, **13**, 2056–2067.
- 12 J. P. F. Lagerwall, P. Rudquist, S. T. Lagerwall and F. Gießeslmann, *Liq. Cryst.*, 2003, **30**, 399–414; J. P. F. Lagerwall, D. D. Parghi, D. Krüerke, F. Gouda and P. Jägemalm, *Liq. Cryst.*, 2002, **29**, 163–178.
- 13 D. R. Medeiros, M. A. Hale, J. K. Leitko and C. G. Willson, *Chem. Mater.*, 1998, **10**, 1805–1813; M. A. Hale, D. R. Medeiros, K. D. Dombrowski and C. G. Willson, *Chem. Mater.*, 1999, **11**, 2515–2519; I. Nishiyama, J. Yamamoto, J. W. Goodby and H. Yokoyama, *Liq. Cryst.*, 2002, **29**, 1409–1423; Y.-I. Suzuki, T. Isozaki, S. Hashimoto, T. Kusumoto, T. Hiyama, Y. Takanishi, H. Takezoe and A. Fukuda, *J. Mater. Chem.*, 1996, **6**, 753–760.
- 14 C. V. Yelemaggad, S. A. Nagamani, G. G. Nair, D. S. S. Rao, K. Prasad and A. Jakli, *Liq. Cryst.*, 2002, **29**, 1181–1185.